



Nonsymmorphic band sticking in a topological superconductor

Yundi Quan

Department of Physics, University of Florida, Gainesville, Florida 32611, USA;
Department of Materials Science and Engineering, University of Florida, Gainesville, Florida 32611, USA;
and Quantum Theory Project, University of Florida, Gainesville, Florida 32611, USA

Valentin Taufour  and Warren E. Pickett 

Department of Physics and Astronomy, University of California Davis, Davis, California 95616, USA



(Received 6 October 2021; revised 10 February 2022; accepted 11 February 2022; published 28 February 2022)

Single-crystal x-ray diffraction recently identified the space group of the weakly correlated yet exotic time reversal symmetry (TRS) breaking superconductor LaNiGa_2 to be nonsymmorphic $Cmcm$. This symmetry causes band sticking on a zone face pierced by four Fermi surfaces, leading to two nodal Fermi lines and a nodal Fermi loop on that zone face $k_z = \frac{\pi}{c}$. These line singularities are examples of perfectly flat (in energy and in geometry) nodal structures that lie precisely at a single energy, with that energy being the Fermi level E_F , even under variation of the carrier density. Projections onto surfaces perpendicular to that zone face produce collapsed drumhead state regions of zero area on the edges of the surface Brillouin zone. Although small by most measures, spin-orbit coupling splits the line and loop degeneracies on the Fermi surfaces (FSs) in the normal state except at two symmetry-related Dirac points, which topologically are locally dispersionless in one direction (zero velocity and infinite mass) while linear in the other two directions. The band sticking and distinctive Fermi surface placed Dirac points are most impactful in establishing LaNiGa_2 as a topological superconductor in the bulk, with the degenerate FSs providing a natural platform for the superconducting order-parameter symmetry necessary for describing this TRS breaking superconductor. Unlike most other crystal symmetries, spin-orbit coupling leaves intact a nodal line piercing the FS, resulting in Dirac points situated at E_F lying along nodal lines. Additionally, the degeneracy exactly at the Fermi energy is central in placing LaNiGa_2 precisely at a Lifshitz FS instability, independent of band filling and protected by $Cmcm$ symmetry. The eight-band low-energy Bogoliubov–de Gennes quasiparticle spectrum is presented along one dispersive direction for varying strengths of TRS breaking. We include a discussion of energetics of gauge symmetry and magnetic order resulting from TRS breaking, incorporating information from experimental data. These results suggest a scenario where TRS breaking rather than gauge-symmetry breaking (superconductivity) might be the driving order parameter.

DOI: [10.1103/PhysRevB.105.064517](https://doi.org/10.1103/PhysRevB.105.064517)

I. INTRODUCTION

The relationship of structure to properties of crystalline materials is a long-running paradigm, especially in solid-state chemistry but also in materials physics. The relation is, however, an involved one: Seemingly closely related, isostructural compounds can show very different behaviors: conducting versus insulating, superconducting versus not, magnetic versus no magnetism, and so on. One example is UPt_3 versus isovalent and isostructural UPd_3 . The former is a heavy fermion superconductor with an exotic pairing symmetry, while the latter is simply a standard normal, nonsuperconducting metal. The broad reason for these bad actors is clear: thermodynamic and other low-energy properties are sensitive to details of the band structure and interactions, hence indirectly to the chemistry and interatomic coupling. In UPt_3 , the U $5f$ states are itinerant with complex Fermi surfaces (FSs) [1], in UPd_3 they are localized with a few simple FSs [2]—great qualitative differences due to the sensitivity of the $5f$ shell to subtle differences in atomic chemistry, size, and electronic coupling.

Early in the 20th century, the impact of degeneracies in Hamiltonians in general [3,4] and electronic structures in particular [5–7] began to be illuminated. In this century, a new aspect of electronic structure has been discovered and pursued intensively—the topological character of the wave functions of occupied electronic bands and the crucial role played by degeneracy. Conventional band crossings that have been neglected over decades of proliferating band structures are being shown to comprise points [8] or form loops [9,10] in the zone that possess topological indices. These in turn guarantee unusual characteristics of certain crystalline properties. Many of these do not influence bulk properties but provide gapless boundary states—Weyl point derived Fermi arcs [8], nodal loop drumhead states—with given types of polarization (symmetry breaking).

In this paper, we focus on LaNiGa_2 , recently established [11] to have a nonsymmorphic space group $Cmcm$ (No. 63) rather than the earlier suggested [12] symmorphic $Cmmm$ (No. 65) space group. While this difference of similar structures may have only a quantitative influence on most normal-state metallic properties, the primary impact arises

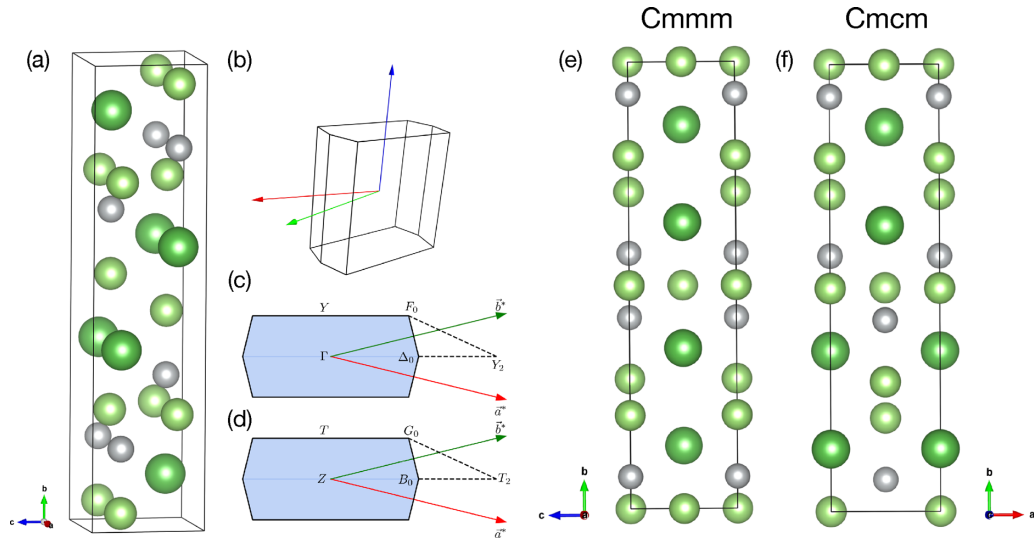


FIG. 1. (a) Oblique view of the crystal structure of LaNiGa₂ in *Cmc* space group. The cell shown is displaced from that in (f) by $\bar{b}/2$. (b) Brillouin zone of LaNiGa₂ in *Cmc* space group, (c) high-symmetry points on $k_z = 0$ plane, (d) high-symmetry points on $k_z = \pi/c$ plane. The high-symmetry k points are Γ : (0,0,0), Y : (0,1,0), F_0 : (0.45,1,0), Δ_0 : (0.53,0,0), Z : (0,0,0.5), T : (0,1,0.5), G_0 : (0.45,1,0.5), B_0 : (0.53,0,0.5), in units of conventional reciprocal lattice vectors. (e), (f) Comparison of the two crystal structures, as labeled. The difference is due to the relative positioning of the two Ni layers (gray spheres) in the center of the figures. The large dark green spheres are La, medium-sized light green spheres are Ga.

because LaNiGa₂ is a superconductor (SC), and an exotic one, in spite of being a simple *s-p* Fermi liquid metal. A previous paper has demonstrated [11] the very substantial effect that the nonsymmorphic band sticking has on the FS and hence on the superconducting order parameter (OP) (gap function). Superconducting LaNiGa₂ displays in μ SR experiments a spontaneous magnetic field that reveals time-reversal symmetry (TRS) breaking [13] with its accompanying magnetization. Current understanding [14] indicates a nonunitary, TRS-breaking OP that needs review in light of the nonsymmorphic space group of the LaNiGa₂ crystal structure.

We address in our paper the detailed electronic structure of LaNiGa₂ and its implications, with emphasis on the effects of nonsymmorphic symmetry. The crystal structure and theoretical methods are described in Sec. II. An earlier paper [11] presented selected results. The electronic structure is presented in Sec. III, where we point out that the Ni 3*d* bands are filled, leaving *s-p* states of all atoms near the Fermi level (E_F) (with some hybridization with Ni 3*d* orbitals). Thus, strong correlation physics does not apply; conventional band theory will give a reliable band structure. The nonsymmorphic group operations lead to band degeneracies (band sticking) across an entire face of the Brillouin zone (BZ) and FSs pierce this wall of degeneracies. A more general description of band degeneracies in orthorhombic crystals has been provided by Leonhardt *et al.* [15]. The band energetics of TRS and gauge symmetry breaking are confronted in Sec. IV. Low-energy models of the electronic degeneracies and the platform for superconducting pairing is the topic of Sec. V. This characteristic, together with spin-orbit coupling (SOC) effects and comparison with the previously suggested structure, provide the focus of our paper. The characteristics of the nonunitary Bogoliubov–de Gennes (BdG) quasiparticle (QP) spectrum are presented in Sec. VI. Section VII provides a summary.

II. STRUCTURES AND METHODS

The nonsymmorphic *Cmc* crystal structure and BZ of LaNiGa₂ are shown in Figs. 1(a) and 1(b). This structure was obtained recently from single crystal x-ray diffraction [11] and is compared to the earlier suggested *Cmmm* structure in Fig. 1(e). In many respects, the structures have several similarities. A layering picture of the structure is natural to apply to both. Both are centered orthorhombic crystals with three-dimensional (3D) electronic structures (see Sec. III). Atomic coordination is similar and the point group D_{2h} is the same. The reported *a* and *c* lattice parameters are nearly identical. Yet there is a fundamental difference.

The difference lies in the relative positions of the two Ni layers separated by Ga, at the center of the diagrams. In *Cmc*, one layer is displaced from the other by $(\frac{1}{2}, 0, \frac{1}{2})$, related by a glide plane instead of a mirror plane. The *z* positions of the Ni layers in *Cmc* differ from those in *Cmmm* by only 0.02 Å. The differences in other atomic positions are smaller (negligible). The crystal symmetry, as we will see, is the crucial distinguishing characteristic. In the orthorhombic *Cmc* symmetry of LaNiGa₂, all atoms lie at Wyckoff 4*c* sites with $m2m$ local symmetry, with special (symmetry dictated) *x* and *z* coordinates. These coordinates, and the unrestricted *y* coordinates, are listed in Table I.

Based on experimental data, the *Cmc* structure supplants in our single crystals the earlier *Cmmm* identification because it predicts correctly several of the rather weak x-ray diffraction spots not present for the *Cmmm* structure. Theory can address the difference directly by comparing total energy of the structures. For both structures, we consider the lattice constants fixed at the experimental values (see the caption of Table I), relax the internal parameters, and calculate the energies on good *k*-point meshes. We find that the energies

TABLE I. Atomic positions of $Cmcm$ LaNiGa_2 , determined by single crystal x-ray diffraction [11]. The lattice constants are $a = 4.278 \text{ \AA}$, $b = 17.436 \text{ \AA}$, $c = 4.271 \text{ \AA}$.

Atom	x	y	z
La	0.0	0.3903	0.75
La	0.0	0.6097	0.25
Ga1	0.5	0.2494	0.75
Ga1	0.5	0.7506	0.25
Ga2	0.5	0.4594	0.25
Ga2	0.5	0.5406	0.75
Ni	0.5	0.3216	0.25
Ni	0.5	0.6784	0.75

are very similar, not surprising because the cells and coordinations are so similar. The $Cmmm$ energy is 12.7 meV/atom lower than that of the $Cmcm$ structure. This energy difference converts to 150K/atom, small compared to the initial heating of constituents. We suggest that some configuration during the slow cooling leading to single crystals favors a free energy of the $Cmcm$ structure, which then gets frozen in. Our calculation is for perfect crystals at $T = 0$ and probably within the accuracy of DFT for this s - p metal. Our samples may therefore be metastable at low T , a situation that is not uncommon amongst polymorphs with similar energies. See, for example, the study of Hinuma *et al.* [16] that addresses such issues.

The linearized augmented plane-wave code [17] WIEN2K was used to obtain density functional based electronic structures, using the generalized gradient functional for exchange and correlation. The atomic sphere radii (R) were, in Bohr: La, 2.50; Ni, 2.40; Ga, 2.12. A plane-wave cutoff K_{max} was obtained from $R_{\text{min}}K_{\text{max}} = 7$ ($R_{\text{min}} = 2.12$ Bohr), and a $14 \times 14 \times 14$ k -point mesh was used for self-consistency. Finer k -point meshes were used in the analysis.

III. RESULTS

A. Electronic structure without SOC

The band structure near the Fermi level E_F of $Cmcm$ versus $Cmmm$ LaNiGa_2 is shown in Fig. 2, along the same symmetry lines. The one for $Cmmm$ is the same as reported previously [18–20]. The two sets of bands have overall similarities but are significantly different in detail. Differences will be due to the difference in Ni layer positioning (see Fig. 1) and related differences in the crystal symmetry. In both cases, the filled Ni 3d bands lie at the same energy, centered near -2 eV with a bandwidth of 1.5 eV.

There are several electron bands just touching E_F along lines in the basal plane (left five panels) for the $Cmmm$ bands. Those features are gone in $Cmcm$, with only two hole bands just touching E_F . There are other bands crossing E_F in both cases, which results in similar values of the Fermi level density of states (DOS) $N(E_F)$, which is 6.5 states/eV—formula unit—both spins for $Cmcm$. A flat band in the $Cmmm$ basal plane (left half of plot) lies around -0.4 eV. That flat band is missing in the $Cmcm$ bands due to band shifts as large as several tenths of an eV and differences in hybridization.

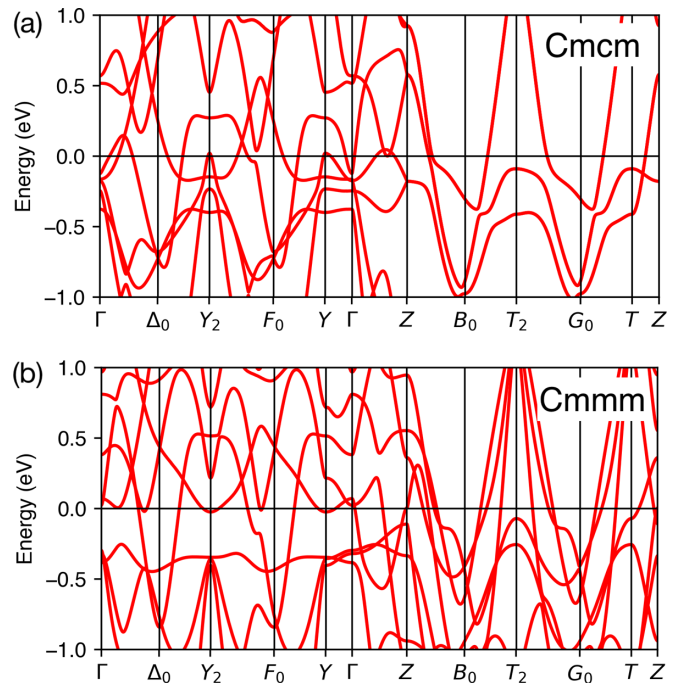


FIG. 2. Band structure plots of nonsymmorphic $Cmcm$ (above) versus symmorphic $Cmmm$ LaNiGa_2 (below) on a 2 eV scale centered on E_F . Note that the nonsymmorphic operation makes the bands stick together on the $k_z = \pi$ plane (which are the right-hand five subpanels in these plots), so the band structure there appears much simpler. Fermi level band crossings are different for $Cmcm$, resulting in different Fermi surfaces (shown earlier by Singh [18] and by Hase and Yanagisawa [19]).

Despite what might be called a lower symmetry structure, the $Cmcm$ bands are simpler due to the nonsymmorphic glide plane operation while the point group is the same. This symmetry operation leads to sticking together of bands across the entire BZ face $k_z = \frac{\pi}{c}$ [top face in Fig. 1(b)]. The corresponding energy bands are twofold orbitally degenerate as well as spin degenerate.

The nodal line *directly along the FS* is profound but simple to picture. The nodal surface (without SOC) is guaranteed by the screw axis symmetry [11]. Depending on the number of screw axis symmetries, many space groups possess one, two, or even three nodal surfaces. With SOC, the nodal line (Z - T) is guaranteed by a combination of inversion symmetry P , the screw axis, and a mirror plane [11]. Many space groups possess these necessary symmetries. The FS, on the other hand, is never guaranteed to intersect the nodal surface or the nodal line. However, when the FS(s) cross the nodal surface, there will be a nodal line independent of E_F until the FS and nodal surface no longer intersect.

While nodal lines in band structures have been found to be common (found in aluminum [9,10]), having a line of degeneracies lie precisely on the Fermi surface is rare (it seems mathematically to have zero probability) and has real impact on properties, and it requires some underlying symmetry. The next most impactful nodal loops are those in semimetals that simply cross the Fermi level [21], such as in the CaAs_3 class [22]. The first reported nodal loop pinned to the FS (i.e., flat

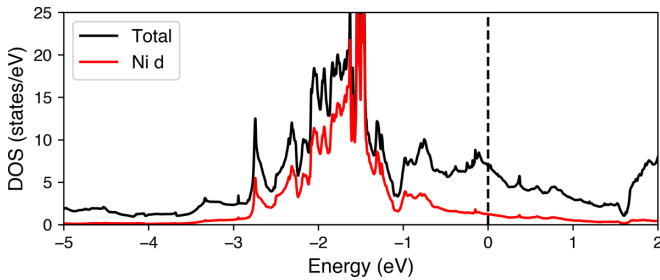


FIG. 3. Density of states of $Cmcm$ LaNiGa_2 . The van Hove singularity below E_F might become relevant in hole-doped samples.

in energy) was located on a zone plane associated with mirror symmetry, discovered by Pardo and Pickett in SrTiO_5 - SrVO_3 layered nanostructures. In that system, orbital ordering and half metallicity played roles in isolating the topological V $3d$ bands [23].

The DOS of $Cmcm$ LaNiGa_2 is presented in Fig. 3. The large peak centered at -1.75 eV and 1 eV wide is the Ni $3d$ band peak, and confirms that the $3d$ bands are filled. E_F lies in a region of modestly declining DOS, about 0.2 eV above a van Hove singularity peak.

B. Electronic structure with SOC

Hase and Yanagisawa [19] have shown the small effect of SOC in $Cmmm$ LaNiGa_2 . However, splittings of degeneracies and some avoided crossings must be looked at because the superconducting energy gap is less than 1 meV. The bands crossing the plane of degeneracies are high velocity s - p states at E_F . While SOC splittings may range up to 40 meV, the inter-Fermi surface separations in k space near the wall (due to SOC) can be very small due to the high velocity. These close encounters may cause magnetic breakdown in magneto-oscillation experiments.

With one exception, SOC splits the fourfold symmetries across the wall of degeneracies and along all the bordering symmetry lines, determined by comparing plots with and without SOC in Fig. 4. The sole symmetry line where SOC does not split the degeneracies is along Z - T . Thus, for the bands that cross the plane of degeneracies along Z - T , SOC does not remove degeneracy at that point.

It becomes relevant for the superconducting state and for topological character that two (symmetry related) fourfold degenerate diabolical (gapless) points remain in the spinful case. The gap opens linearly away from the Z - T line: Dispersion is massless along both perpendicular directions, which can be considered as four Dirac particle bands with two (anisotropic) velocities. As mentioned, the bands remain degenerate along Z - T . Topological aspects of nodal loops in the presence of SOC were studied by Allen [9,10] in his re-discovery of nodal lines in this century. We return to this issue in Sec. IV.

To illustrate the effects of SOC on the $k_z = \frac{\pi}{c}$ plane, we have calculated the band splittings due to SOC on a fine mesh. There are four (eight if spin degeneracy is included) bands that cross the Fermi level, see Fig. 4. The right five columns of these figures illustrate the sticking together of bands on

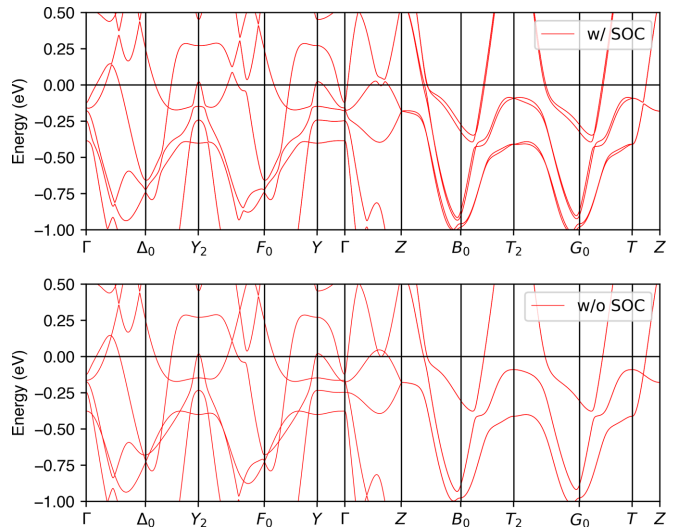


FIG. 4. Band structure of LaNiGa_2 with (above) and without (below) spin-orbit coupling. Effects of SOC are small but important, as discussed in the text. Note especially the lack of splitting along T - Z .

this plane due to the nonsymmorphic space group. This figure indicates the magnitude of SOC splitting along several symmetry lines. Figure 5 provides a view of the constant energy surfaces on the degeneracy plane ($k_z = \pi/c$ plane), including splittings due to SOC. Leonhardt *et al.* pointed out the special aspects of band degeneracy in space group $Cmcm$ [15].

C. Fermi surfaces and nodal features

The FSs of LaNiGa_2 are shown in Fig. 6; SOC effects would not be visible in this plot. There are five FSs, with FS1 being rather small, comprised of a pair of complex shaped columns on either side of Γ . The other four FSs are constituted of two pairs of large open surfaces, each pair being locked together by the nonsymmorphic operation on the plane of degeneracies. FS2 and FS3 are large sheets that meet to form a single nodal loop in the shape of a rounded rectangle lying on the $k_z = \pi/c$ zone boundary. Due to degeneracy, these surfaces have similarity of shape near the loop. FS4 and FS5 are fluted (quasi-2D) Russian doll cylinders at the zone corners that meet to form a pair of symmetry related FS4/FS5 open nodal lines that extend across the degeneracy plane in passing from one BZ to the next. The full FS in Fig. 5 shows that the loop and lines almost intersect, but have small anticrossings due to band hybridization on the degeneracy plane. See also Fig. 7.

The FS2/FS3 nodal loop crosses the Z - T line where SOC does not lift degeneracies. Elsewhere, SOC lifts degeneracies and the nodal lines and nodal loop are gapped except at the intersection of the loop with the symmetry line Z - T , where two nodes persist. At these points, LaNiGa_2 hosts fourfold massless (Dirac) fermions pinned at E_F , an unusual occurrence of topological interest. These Dirac points, surviving SOC and pinned to the Fermi energy independent of carrier concentration, play a pivotal role in the following discussion.

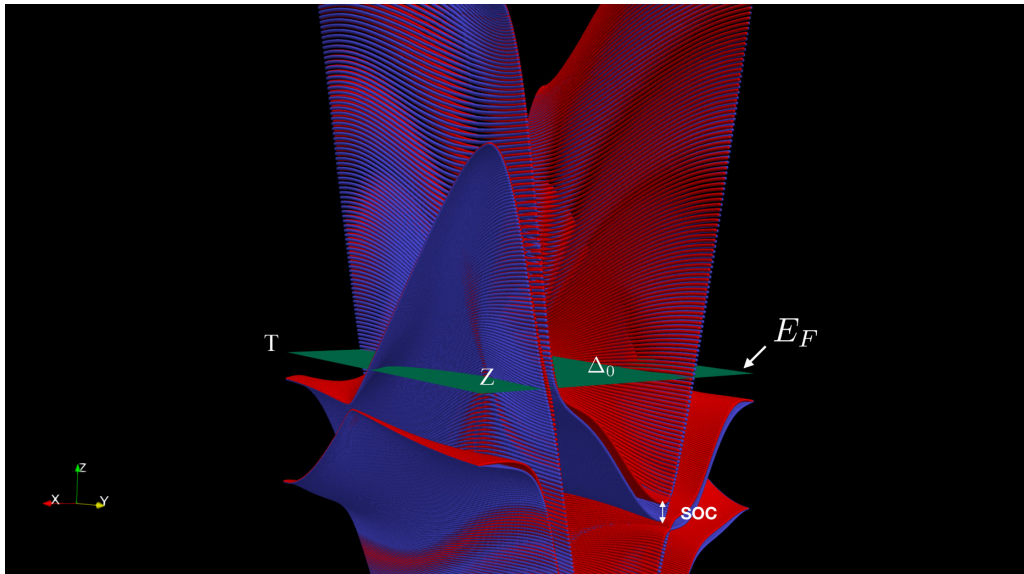


FIG. 5. Energy surface plot for *Cmc* LaNiGa₂ on the $k_z = \pi/c$ plane, with the $Z - T$ line indicated. The intersection of various bands with the Fermi energy E_F can be seen. The Dirac band touching point is identified by the small vertical arrow. The small SOC splitting is visible between nearby bands in several places. Along the $T - Z - T$ line, SOC splitting vanishes, leaving the Dirac points as the only true degeneracies. Also evident from the figure is the combination of bands near the nodal point with very small, moderate, and large velocities—a highly anisotropic electronic structure.

D. Surface projections and surface states

In the absence of SOC, such nodal loops and lines are spin degenerate and topological: Integration of the Berry connection along a contour surrounding a loop or line gives a Berry phase [9,10,24,25] of $\theta = \pm\pi$ for either spin. When projected onto a sample surface, the loops (or lines) normally give rise to real-space surface-localized drumhead states within the projection, which is a closed contour.

For LaNiGa₂, two of these projections are anomalous because the loop and lines lie along a zone face, i.e., on a plane

(flat surface) perpendicular to two surfaces, see Fig. 7. Projection onto these sample surfaces give straight lines along an edge of the surface BZ edge. These singularities are diabolical in a new sense: the drumhead state area vanishes, leaving a straight line of singular behavior with δ -function width, as illustrated in Fig. 7 (near corner and top plane). The surface zone parallel to the plane of degeneracies (front face in Fig. 7) will surround drumhead states in a conventional fashion.

SOC alters θ from this quantized value by lifting the degeneracy and thereby removing the topological nature. θ does not

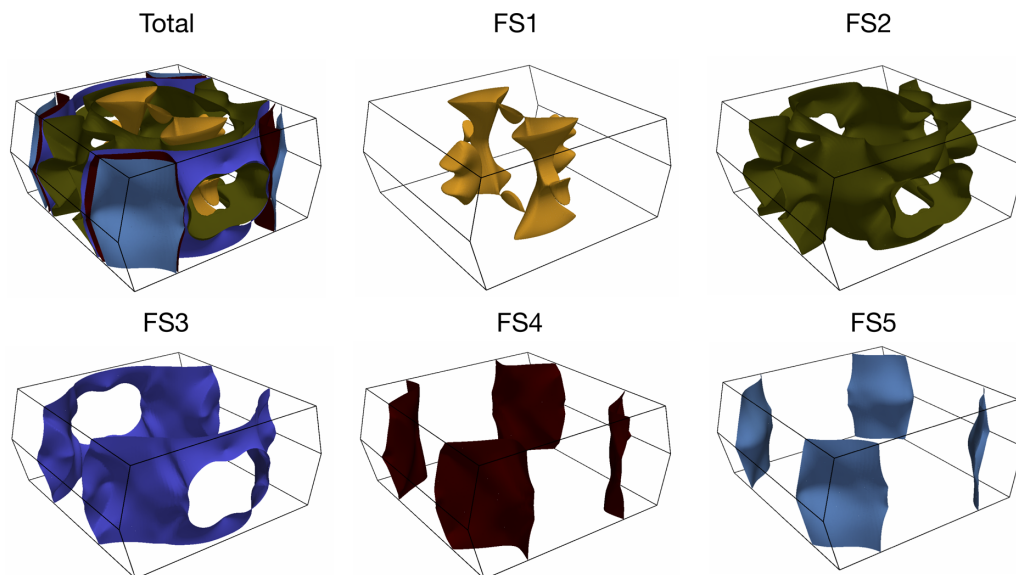


FIG. 6. Fermi surfaces of LaNiGa₂ in *Cmc* structure. The pairs FS2/FS3 and FS4/FS5 are degenerate along the plane of degeneracies (the front right edge).

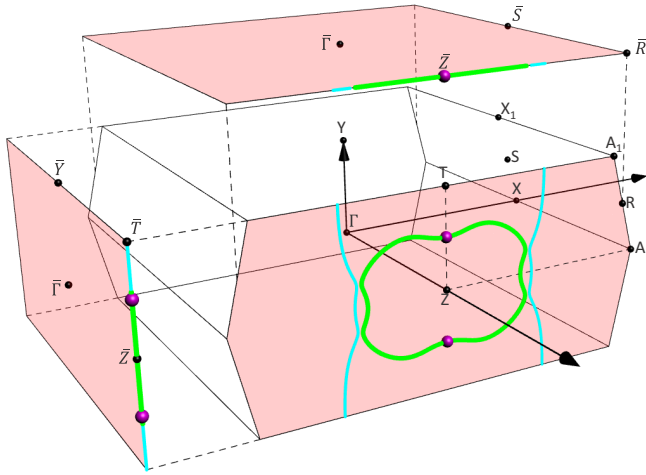


FIG. 7. Projection of nodal lines at the Fermi level onto surface Brillouin zones (pink planes) for each of the Cartesian axes. Green (blue) denotes the loop (lines) and their projections. The magenta dots indicate the position of the Dirac points surviving SOC. Note that the left and upper projections contain no area.

vanish, instead (as shown by Allen [9]) it becomes dependent on the strength of SOC and the contour of integration around the point [9,10]. See, however, the discussion of the special (Dirac) point, below. With SOC, the edges of the drumhead states are no longer precisely defined, and confinement to the surface will no longer be exponential. This SOC detail has more importance for the superconducting OP because the superconducting gap is small compared to effects of SOC.

IV. DIRAC POINTS SURVIVING SOC

As mentioned above, when SOC is included, degeneracies are lifted on the $k_z = \frac{\pi}{c}$ plane *except* along the Z - T line. This leaves two Dirac points \vec{k}_D , symmetrically placed across Z , where the FS nodal loop intersects the Z - T line. The twofold band degeneracy assures that these two k_D points are diabolical, and here we establish them as generalized Dirac points, with distinctive topological character.

The two bands, pictured in Figs. 8(a)–8(c), at low energy can be represented with respect to k_D in terms of (band or orbital) Pauli matrices τ_j , $j = 0, 3$ as

$$\hat{\epsilon}_k = g_{0,k}\tau_0 + g_{1,k}\tau_1 + g_{2,k}\tau_2 + g_{3,k}\tau_3, \quad (1)$$

where $g_{j,k}$ are real expansion functions. $g_{0,k}$ is simply the mean energy of the two bands, smooth and not affecting the topological properties, so we subtract it out to study the topological nature. The eigenvalues (relative band energies) are $\epsilon_{n,k} = \pm(g_{1,k}^2 + g_{2,k}^2 + g_{3,k}^2)^{1/2}$, $n = \pm$, pictured in Figs. 8(d)–8(f), and they vanish at \vec{k}_D (the panel center).

Fitting this form to the calculated values and using the coordinate system of Fig. 7 leads to linear bands along the k_x and k_z directions, and dispersion along k_y corresponding to zero (Pauli) velocity (zero linear term, see below) and infinite mass (zero quadratic term). In fact, all higher order terms vanish as well, due to the Z - T degeneracy. The pair of linear directions remind us of an anisotropic Dirac point, but zero dispersion along the third axis gives a type of diabolical

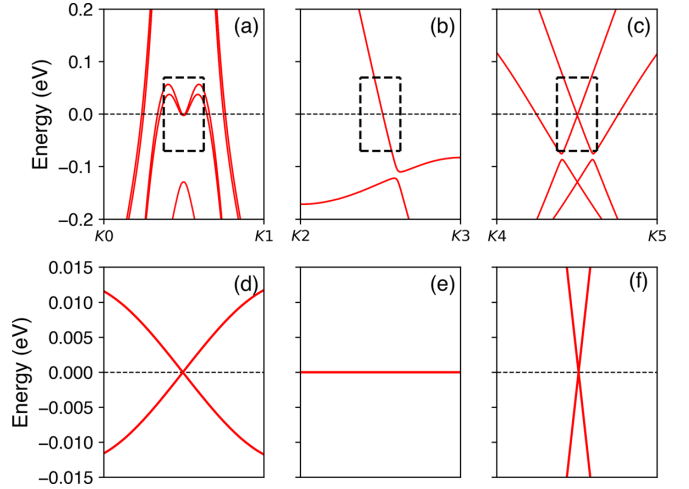


FIG. 8. Dispersion in three directions through the Dirac point on the Z - T line, when SOC is included: (a) k_x direction, in the $k_z = \frac{\pi}{c}$ plane, (b) k_y direction, along Z - T , (c) k_z direction. The point \vec{k}_D lies at the center of each panel. A Pauli matrix representation (in band space) has been used to represent the dispersion near the Dirac point. In the bottom panels, the Pauli σ_0 term has been subtracted out, revealing the Dirac point plus flat dispersion character. K0 $(-0.5, 0.516, 0.5)$, K1 $(0.5, 0.516, 0.5)$, K2 = Z $(0,0,0.5)$, K3 = T $(0,0.5,0.5)$, K4 $(0, 0.516, 0.4)$, K5 $(0, 0.516, 0.6)$.

point whose topological nature requires addressing. The Pauli velocities v^P , which give the splitting of the bands upon leaving the line of degeneracy and are shown in Figs. 8(d)–8(f), are $v_x^P = 6 \text{ meV \AA}$, $v_y^P = 0$, $v_z^P = 25 \text{ meV \AA}$, with the zero velocity being along the k_y (Z - T) line of degeneracies, which is the special direction for the algebra below. The bands spread slowly in leaving \vec{k}_D in the other two directions because of the small SOC. The physical velocities have contributions from $g_{0,k}$ and are more typical band velocities.

A. The topological character

For notational simplicity, we introduce $\kappa_x = v_x^P(k_x - k_{D,x})$, etc., i.e., the scaled separation from the Dirac point. The distance along κ_y will not appear, so it simply represents the third coordinate. The low-energy character can be obtained for small $\vec{\kappa}$ as

$$\mathcal{E}_\kappa = \kappa_z\tau_1 + \kappa_x\tau_2, \quad (2)$$

with no dependence on κ_y . [The subscripts on the (band) Pauli matrices do not refer to Cartesian directions.] In the 3D space of $\vec{\kappa}$, the constant energy \mathcal{E} surfaces are given by (i) along direction κ_y : $\kappa_z = \pm\sqrt{\mathcal{E} - \kappa_x^2}$, when the argument is non-negative; these are touching cones surrounding the κ_y axis; (ii) along κ_x , where $\kappa_y = \kappa_z = 0$, $\kappa_x = \pm\sqrt{\mathcal{E}}$, a pair of constant κ_x planes (locally), and (iii) along κ_z , an analogous pair of planes. This is a generalization of the graphene Dirac point in which κ_y enlarges the space but plays no part in the dispersion (as would k_z in graphene).

The Berry connection obtains no contribution from the planes. The cones give rise to a graphenelike singularity with an important difference: The singularity lies not at the 2D origin—the Dirac monopole singularity of graphene—but

rather along the k_y line $\kappa_{\perp} = 0$, where $\kappa_{\perp} = \sqrt{\kappa_x^2 + \kappa_z^2}$. The point \vec{k}_D is the special point (source) of the Berry connection calculated from the occupied eigenket $\frac{1}{\sqrt{2}}[1, -e^{i\phi}]^T$. In spherical coordinates (effectively polar coordinates here), the nonzero component is

$$\begin{aligned}\vec{A}_{\phi} &= i \langle k, - | |\nabla_k| | k, - \rangle \\ &= i \left\{ \frac{1}{\sqrt{2}}[1, -e^{-i\phi}] \frac{1}{\sqrt{2}} \frac{i}{\kappa_{\perp}} [0, e^{i\phi}]^T \right\} = \frac{1}{2\kappa_{\perp}}.\end{aligned}\quad (3)$$

Here $\phi = \tan^{-1} \frac{\kappa_x}{\kappa_z}$ is the polar angle with respect to the k_y axis. \mathcal{A}_{ϕ} is the only nonzero component: \vec{A} is circulating vector field with amplitude $1/2\kappa_{\perp}$. The circuit integral of \mathcal{A} at radius κ_{\perp} is

$$\oint \vec{A} \cdot d\vec{k} \rightarrow \int_0^{2\pi} \mathcal{A}_{\phi} \kappa_{\perp} d\phi = \pi, \quad (4)$$

independent of the circuit radius. Thus, point \vec{k}_D , and in fact the entire line Z - T of degeneracies carries a Berry phase of π , even for radius $\kappa_{\perp} \rightarrow 0$. This is expected for a nodal line of degeneracies, but in this case the line is stuck onto the BZ face by nonsymmorphic $Cmcm$ symmetry. Allen showed that, barring exceptional occurrences, SOC causes deviation of the Berry phase of π to a value that is dependent on contour and SOC strength [9,10]. The exercise above demonstrates that nonsymmorphic symmetry operations can provide an exception to this rule, retaining the nodal line and Berry phase of π even upon inclusion of SOC.

B. A different topological peculiarity

Returning to the physical bands in Figs. 8(a)–8(c), a different aspect of topology becomes evident. The bands pictured in Fig. 8(a) reveals that the Dirac point is a minimum in the band energies along the k_x axis, that is, perpendicular to the nodal loop along the plane of degeneracies $k_z = \pi/c$ where band separation is due solely to SOC. A decrease in the energy \mathcal{E} below E_F gives no surface at \mathcal{E} along this direction through \vec{k}_D , while an increase above E_F gives four \mathcal{E} surface crossings (pairs symmetrically placed) for the two bands. The position of E_F therefore places LaNiGa₂ at a Lifshitz instability, in which the constant energy surface changes topology in going from above E_F to below. Varying the carrier concentrations (i.e., E_F , only changes the energy, but retains E_F as the point of instability. An actual instability can only be accommodated by breaking of the nonsymmorphic symmetry.

LaNiGa₂ therefore resides at a position of instability. Lifshitz transitions are typically important when carrier density shifts E_F across the band edge or when a parameter (pressure, strain, temperature) shifts the band edge across E_F . The situation here is different: This Lifshitz band edge follows (in energy) changes in E_F , with related shifts of \vec{k}_D along the Z - T line. This situation of E_F exactly at a band edge may impact transport and other low-energy properties exaggerated by proximity to an electronic instability, but pins the chemical potential as an instability point.

A Lifshitz transition may involve structural responses that would disrupt the nonsymmorphic symmetry of LaNiGa₂. The impact of this incipient instability lies beyond the scope

of this paper. Among other considerations, in LaNiGa₂ it affects a limited region of the (large) FSs in LaNiGa₂, making its impact challenging to quantify. For a nonsymmorphic semimetal where the entire FS may be affected by the loss of a symmetry operation, the impact is worthy of further study.

V. ENERGETICS OF BROKEN SYMMETRIES

The pairing interaction(s) leading to exotic superconducting states are an open topic, so there has been very limited discussion of relative energetics in real materials. A common view, based on surveys of the classes of exotic superconductors, is that low energy spin or charge fluctuations guide symmetry breaking, with pair fluctuations leading to superconducting order competing with spin or charge density waves [26,27]. Since there is no indication from the electronic structure of such fluctuations with significant strength, LaNiGa₂ provides a promising platform for the importance of orbital fluctuations. See Sec. VI for more discussion of the proposed pairing symmetry of LaNiGa₂.

In model Hamiltonian studies or gap equation solutions, the energetics of competing phases is the central property in determining a phase diagram. Results can be sensitive to the interactions that are included, the values of parameters, cutoffs to eliminate the higher energy states, and to what extent fluctuations are accounted for. Here a few observations on relative energetics of LaNiGa₂ are provided, incorporating experimental and electronic structure data.

For $T_c = 2\text{K}$, $k_B T_c = 0.17$ meV. The calculation gives $N(E_F) = 6.5$ states/eV-f.u. From Ghosh *et al.* [14], $\Delta_o = \Delta(T=0) \approx 1.5 k_B T_c = 0.25$ meV, which is close to the BCS weak-coupling relation for the gap $2\Delta_o = 3.5 k_B T_c = 0.60$ meV. In BCS theory [28,29], the net energy gain in the ground state (superconducting condensation energy) is $\Delta E_{sc} = \frac{1}{2} N(E_F) \Delta_o^2 \sim 0.2 \mu\text{eV}$.

From the μSR data of Ghosh *et al.* [14], the observed internal field $B_{\text{int}} = 0.3$ G, corresponding to a TRS-breaking magnetic moment of $m = 0.012 \mu_B/\text{f.u.}$ The associated energy (exchange-kinetic) gain from standard magnetic band theory [30] is $\Delta E_{\text{mag}} = \frac{1}{4} [\frac{1}{2}] I_{\text{St}} m^2 \sim 6 \mu\text{eV}$. Here I_{St} is the Stoner exchange interaction between parallel spins that arises from the exchange-correlation functional. Being primarily an s - p metal at E_F , I_{St} will be of the order of 0.5 eV [31]. This energy gain is a factor of 30 larger than the superconducting condensation energy. So why don't more superconductors show TRS breaking?

This expression is based on a Stoner-like mechanism of ferromagnetism, and LaNiGa₂ is well away from a Stoner instability. Thus, this energy is not a gain but rather the *cost* in energy in enforcing the moment m onto the system. Being unfavorable and roughly 30 times larger than the attractive condensation energy provides a conundrum: How is this large cost in magnetic energy accommodated?

Another relevant comparison is the SC gap versus the spin-exchange splitting that splits up and down spin bands, which is given by

$$\Delta_{\text{ex}} = \frac{m}{N(E_F)} = \frac{0.012}{6.5/\text{eV}} = 1.85 \text{ meV}. \quad (5)$$

The SC gap of 0.60 meV is three times smaller, so spin-singlet pairing would be strongly opposed by an exchange splitting larger than the gap. This observation, together with the energetics above, suggest spin magnetism may not be the origin of the magnetic field experienced by muons or that triplet-spin pairing emerges in LaNiGa₂ with energetics different from BCS.

One scenario is that the SC mechanism is different from BCS singlet spin-pairing, although the phenomenology may be similar. However, since spin polarization as the origin of TRS breaking seems to be energetically unlikely, natural alternatives are (i) band (orbital) polarization, which would involve different energetics on the magnetic side of the comparison, or (ii) spin-triplet (or equal spin) pairing. A confrontation to these alternative pictures is that the gap derived from experimental data is consistent with the BCS spin-singlet value. The next section describes how the nonsymmorphic structure of LaNiGa₂ impacts a proposed nonunitary spin-triplet pairing model. A different means of studying coupled superconducting-magnetic systems is via Ginzburg-Landau free-energy theory. Generalization of the study of Krey [32] to small magnetizations might, however, even in the uniform bulk case, involve several parameter whose values are unknown.

VI. NONUNITARY PAIRING MODEL

Nodal line LaNiGa₂ is unusual in having degenerate pairs of bands pinned at constant energy, lying *precisely at the Fermi level* even if the Fermi level is shifted as, for example, by nonstoichiometry. This is possible in certain nonsymmorphic metals with FSs crossing the BZ face where pairs of bands stick together. Another feature of more interest for the SC phase is that, unlike the case for conventional FSs, direct inter-band transitions (momentum transfer $\vec{q} = 0$) coupling bands persist all the way to zero energy when Dirac, semi-Dirac points or nodal lines are stuck at the Fermi energy. Such degeneracies thereby promote, intrinsically, two-band materials or two-band superconductors.

We review first on the lines and loop of Dirac points at the chemical potential μ (equal to E_F at $T = 0$), neglecting SOC. Specifically, *Cmcm* LaNiGa₂ has two nodal (Dirac) lines on the FS2/FS3 pair, lines that are open in common parlance but closed on the 3D torus due to the periodicity in k space. In addition there is one large closed FS4/FS5 loop. Pairing on the rest of the FS may be treated in the usual manner: the full gap extends across the FS while the low-energy behavior in the SC state is determined by the lines of degeneracy at low energy.

The two-band extension of the internally antisymmetric nonunitary triplet (INT) model pursued by Ghosh *et al.* [14] was based on two Ni orbitals. However, the Ni 3*d* bands are filled and Ni 4*s*-4*p* character at E_F is minor. A more natural picture than Ni orbitals is that the two components besides spin are the two bands that become degenerate on the nodal lines, an interpretation that is only physically relevant due to the nonsymmorphic structure. Due to the identical point groups of *Cmmm* and *Cmcm* space groups, the formalism of the INT model can be adapted directly from that used by Weng *et al.* [33] and Ghosh *et al.* [14] for *Cmcm*.

A. The normal state spectrum around a Dirac point

The BdG Hamiltonian has the form

$$\tilde{\mathcal{H}} = \begin{pmatrix} \mathcal{H}_b(\mathbf{k}) & \tilde{\Delta} \\ \tilde{\Delta}^\dagger & -\mathcal{H}_b(\mathbf{k}) \end{pmatrix}. \quad (6)$$

with the normal state band Hamiltonian around a point node at \vec{k}_D , with chemical potential μ , given by

$$\mathcal{H}_b(\mathbf{k}) = \mathbf{1}_2 \otimes \begin{pmatrix} \delta\epsilon_k - \mu & \vec{\gamma}_k \cdot \delta\vec{k} \\ \vec{\gamma}_k \cdot \delta\vec{k} & -\delta\epsilon_k + \mu \end{pmatrix}, \quad (7)$$

where $\delta\vec{k} = \vec{k} - \vec{k}_D$ and $\delta\epsilon_k = \vec{v}_k \cdot \delta\vec{k}$. This expression captures the normal state band dispersion near the Dirac point when SOC is included (or near the Dirac lines and loop when SOC is not included). This expression does not include a σ_0 term, which is the average of the two bands, because it is irrelevant for the questions of TRS breaking or OP symmetry. Superconductivity, viz. the value of T_c , will depend on the separate velocities (and resulting DOS), and on matrix elements of the pairing potential between bands, but those effects are not part of the current discussion.

The bands near the node are coupled by linear hybridization (the $\vec{\gamma}$ term) since it vanishes at the crossing without other restrictions. \mathcal{H}_b has eigenvalues (we need only consider $\mu = 0$)

$$\lambda_k = \pm\sqrt{\delta\epsilon_k^2 + (\vec{\gamma} \cdot \vec{k})^2} = \pm\sqrt{|v_k^* k|}. \quad (8)$$

For $\mu = 0$, the first effect is to renormalize the anisotropic velocity to $v_k^* = \sqrt{(\vec{v}_k \cdot \hat{k})^2 + (\vec{\gamma}_k \cdot \hat{k})^2}$. The hybridization does, however, provide a second effect: the necessary coupling of the bands.

Over the FS at general points, the small SOC has little effect except to rotate spin-degeneracy to quasispin degeneracy, retaining Kramers degeneracy, and to convert the bands to mixed quasibands.

The behavior near the Dirac points \vec{k}_D determines the low-energy behavior; elsewhere the SOC splitting dominates the small SC gap. Breaking of the fourfold degeneracy by the SC gap is nonperturbative, converting the gapless metal to the gapped superconductor. Pairing is the primary effect, and in LaNiGa₂ accounting for TRS breaking (a coupled OP) is also a discontinuous, nonperturbative change accompanying breaking of gauge symmetry.

B. Exotic pairing and the BdG spectrum

While the gap function may have \vec{k} variation over the FS, what is relevant at the lowest temperatures is the gap operator near the \vec{k}_D points and the gap value(s); slow \vec{k} dependence around the FS can be averaged over and for discussing purposes neglected. The OP structure that has been proposed for TRS-breaking LaNiGa₂ has the form

$$\tilde{\Delta} = (\mathbf{d}_s \cdot \sigma) i\sigma_y \otimes i\tau_y. \quad (9)$$

The tensor product involves the band index for $i\tau_y$ with eigenvalues $m = \pm i$, and the spin (σ matrices) channel $\sigma = \uparrow, \downarrow$, all being degenerate at the Dirac point, taken below to be $\vec{k}_D = 0$, the local origin. The spontaneous vector field \mathbf{d}_s in this form couples to spin like a magnetic moment, enabling

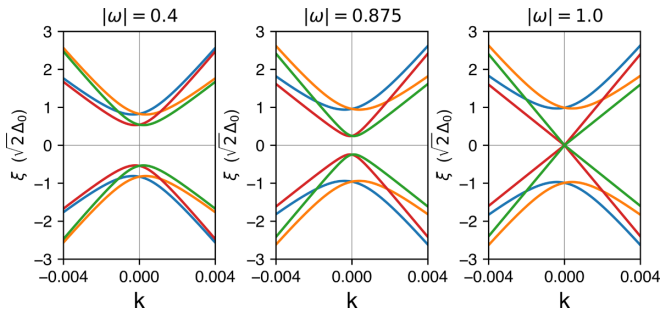


FIG. 9. Schematic Bogoliubov band structure along one dispersive band direction of the triplet, topological superconductivity model for LaNiGa₂. Three values of the triplet strength ω are shown. Note that the nonsymmorphic band-sticking at the zone boundary persists into the superconducting state. Reaching the unitary limit $|\omega| = 1$ results in gapless Dirac quasiparticles at the lowest energies.

TRS breaking due to a spontaneous magnetic polarization. The mechanism of spin-triplet coupling in Fe-based superconductors was suggested by Dai *et al.* [34] to arise from Hund's rule spin alignment, although they explored only TRS preserving forms for \vec{d} . Hund's rule physics is however not expected in an *s-p* metal like LaNiGa₂.

Writing the triplet \vec{d}_s vector as (real positive) pairing amplitude Δ times complex unit vector η leads to $\mathbf{d} = \Delta\eta$. Nonunitarity of the triplet state is characterized by a nonvanishing real vector $\vec{\omega} = i(\eta \times \eta^*)$ which satisfies $\omega \equiv |\vec{\omega}| \leq |\eta|^2 = 1$. The normal state dispersion is linear along two axes and quadratic along the third, as shown in Figs. 8(a)–8(c). This fourfold degenerate (counting spin) semi-Dirac point has an unusual aspect: the pair of massive bands, along k_x , have the same sign but different values. There is no particle-hole symmetry, rather E_F pins the system at a Lifshitz FS instability, protected by *Cmcm* symmetry.

The dispersion ξ_k of the BdG QPs of Eq. (2) is given, in either of the two directions of linear dispersion, by the eight branches

$$\xi_k = \pm \left[\sqrt{\lambda_k^2 + |\Delta|^2(1 \pm |\vec{\omega}|)} \right] \pm \vec{\gamma}_k \cdot \vec{k}, \quad (10)$$

with two gaps $\Delta\sqrt{1 \pm \omega}$. The QP spectrum is shown along an arbitrary direction in Fig. 9 for $\mu = 0$, $v^* = 500$, $\Delta = 0.7$, $\omega = 0.4, 0.875, 1.0$, $\gamma = 100$ for k in the range $[-0.004, 0.004]$. Pairs of BdG QP bands persist in sticking together on both sides of the gap at $k = 0$ (the Dirac point). The QP dispersion will be highly anisotropic, so the gap edge structure may be nearly 2D-like.

The quasiparticle DOS (QPDOS) (for one-dimensional dispersion) in the superconducting state corresponding to the eight bands of Eq. (9) is shown in Fig. 10 for the three same values of triplet strength and two values of broadening (included partially to regularize the peaks). The QPDOS becomes gapped as ω is reduced from unity, developing a two gap (two-band) form that finally merges into conventional single gap form as ω vanishes.

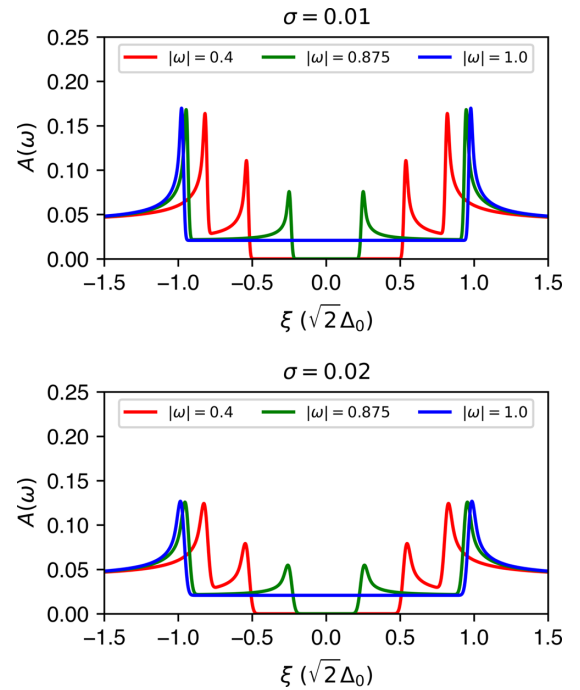


FIG. 10. Quasiparticle density of states for the Bogoliubov–de Gennes bands (see Fig. 9) of the triplet, topological superconductivity model for LaNiGa₂. Three values of the triplet strength ω are shown. Reaching the unitary limit $|\vec{\omega}| = 1$ results in a gapless state.

C. On the driving order parameter

The weakness of the magnetic field reflecting TRS breaking (internal field of 0.3 G, comparable to the earth's field at its surface) and the standard interpretation as spin ferromagnetism raises the question of how spin symmetry could be broken by such a small amount of magnetization ($0.012\mu_B/\text{f.u.}$, about 1/2,500 the magnetization of *bcc* Fe). Considering the isomorphic spaces of spins and bands (or, equivalently, Wannier orbitals), the pairing operator in Eq. (9) can equally well serve with $\vec{d}_s \cdot \vec{\sigma}$ replaced by $\vec{d}_o \cdot \vec{\tau}$. In this form the symmetry-breaking orbital field \vec{d}_o (orbital angular momentum polarization) is directly coupled to the two-orbital space, giving orbital (rather than spin) angular momentum polarization and associated orbital magnetism. This OP would imply orbital currents. In analogy with Dai *et al.*'s suggestion of Hund's spin pairing [34], a type of small- q electron-phonon coupling (see below) that strongly favors intraband over interband coupling would promote this type of orbital triplet pairing.

From a Ginzburg-Landau free energy viewpoint, one treats two individual OPs $\alpha = 1, 2$, being coupled, each having its own (uncoupled) $T_{c,\alpha}^0$. The one with higher T_c^0 can be considered the driving OP, in the sense that it is encountered first upon lowering the temperature, with the other (parasitic) OP tuning T_c and renormalizing other properties. In LaNiGa₂, without appreciable spin fluctuations but clear multi-orbital character at low energy, orbital-(a)symmetry could be the strong candidate as the driving OP, with an associated polarization (i.e., asymmetry) as its observable signature. Connections between isolated Dirac points, TRS breaking, nonunitary OPs, and multi-orbital physics has been discussed

by Lado and Sigrist [35], considering remote Dirac points (i.e., away from the Fermi level) in two dimensions.

Somewhat analogous orbital currents have been suggested in cuprates [36] and indications of observations in related magnetic materials have appeared [37]. This scenario of orbital polarization helps to alleviate the small magnetization conundrum but leaves the mechanism, in physical terms, of TRS breaking (orbital polarization) as a challenging question, as is the case with most TRS breaking superconductors. Non-magnetic s - p LaNiGa₂, however, is fundamentally different from magnetic materials that have served as platforms for formation of orbital currents.

The microscopic mechanism behind exotic superconducting pairing is one of importance, both for a better understanding and for guiding searches for other, perhaps exotic, examples. LaNiGa₂ is seemingly a common s - p Fermi liquid, not a candidate for peculiar broken symmetries. Tütüncü and Srivastava calculated the phonon spectrum, electron-phonon coupling for the Eliashberg spectral function, and T_c (for the $Cmmm$ structure) [20]. They obtained the electron-phonon coupling strength $\lambda = 0.70$, and with a Coulomb pseudopotential $\mu^* = 0.17$ obtained $T_c = 1.9$ K. This value of T_c is in excellent agreement with experimental reports, thus all indications—except TRS breaking—point toward electron-phonon coupling as the underlying mechanism.

This leaves the issue of TRS breaking. In Fe-based superconductors as an example, where Coulomb repulsion (through spin fluctuations) is indicated as the interaction that needs scrutiny, there has been focus on FS scattering between various small pockets. For example, Platt *et al.* argued that three-FS scattering processes can, in certain regimes of parameters, tip the balance from $s + is$ pairing to TRS breaking $s + id$ pairing, thus proposing this as the mechanism promoting TRS breaking in iron pnictides [38]. The five large FSs permeating the BZ in LaNiGa₂ are at the opposite extreme from the small iron pnictide FSs. The distinction in LaNiGa₂ is that nonsymmorphic symmetry-required, nearby in k , FSs around the nodal line must play a role, and they actually touch at the nodal point even in the presence of SOC. These aspects could form the basis of a study of the FS impact on the mechanism and on the form of the gap function.

One point relevant to the driving versus parasitic OP question should be made clear. The form of the OP in Eq. (9) includes the implicit feature that TRS and gauge symmetry are broken together (as in the Ginzburg-Landau treatment). LaNiGa₂ is thus not unstable to simple s -wave pairing alone, although it might be at a somewhat lower temperature (as implied by the Eliashberg calculations mentioned just above, which assumes s -wave pairing). It may be most unstable to—driven by—this, or some, form of TRS breaking OP. These questions remain for further study.

VII. SUMMARY

The electronic structure of LaNiGa₂ has been analyzed in light of the discovery of its $Cmcm$ space group and crystal

structure, different than originally reported. The effect of the nonsymmorphic $Cmcm$ symmetry on the electronic structure of LaNiGa₂ enforces a degeneracy (sticking together) of band pairs on the $k_z = \frac{\pi}{c}$ zone face. The very unusual result—nearly all nodal lines and loops have dispersion—is a pair of dispersionless open nodal lines and large nodal loop on this plane, lying on the line of intersection of the zone face with the FS. The band sticking protects the degeneracies from changes in the chemical potential, and the diabolical features are pinned to the Fermi level.

These factors become more surprising because LaNiGa₂ is at the basic level a simple s - p Fermi liquid (the Ni $3d$ bands are filled) that becomes an exotic topological superconductor below 2 K. The crystal symmetry, finite superconducting gap, and TRS breaking, according to current theory, indicate a triplet, nonunitary OP in the broken symmetry state. It becomes reasonable to consider whether LaNiGa₂ provides an example in which gauge-symmetry breaking (superconductivity) is a parasitic OP, being driven superconducting by a TRS-breaking mechanism.

Whereas SOC lifts degeneracies almost everywhere, there is one zone-face T - Z - T symmetry line where SOC vanishes. Most of the line and loop degeneracy is lifted by SOC, leaving very closely separated FS edges because SOC is small while the band velocity is relatively large. Because the nodal loop crosses this line, LaNiGa₂ is finally left with two semi-Dirac points on the $k_z = \frac{\pi}{c}$ zone face. Their projections on surfaces perpendicular to this zone face contain “collapsed Fermi arcs:” singular lines along the surface BZ edges. The effect of such singularities on physical properties requires further study. The quadratic dispersion from the semi-Dirac point leaves LaNiGa₂ positioned at a Lifshitz instability, protected by $Cmcm$ symmetry.

Some aspects of the energetics of gauge symmetry and TRS breaking have been explored using experimental data. The cost in magnetic (spin) polarization energy is an order of magnitude larger than the gain in condensation energy, seeming to make BCS spin-singlet pairing untenable. The BdG eight-QP-band structure for a two spin, two band, nonunitary triplet spin pairing operator has been presented for varying strengths of nonunitarity. The possibility has been raised that the driving OP for TRS breaking is band polarization with indirect spin polarization, versus direct spin polarization, and that gauge symmetry breaking may be a parasitic OP. We expect that our results will provide an important step forward in the understanding of this exotic, perhaps unique, superconductor.

ACKNOWLEDGMENTS

We thank A. P. Schnyder for useful discussions. Work by Y.Q. utilized the Extreme Science and Engineering Discovery Environment (XSEDE), which is supported by National Science Foundation Grant No. ACI-1548562. V.T. acknowledges funding from the UC Laboratory Fees Research Program (LFR-20-653926). W.E.P. acknowledges support from U.S. National Science Foundation Grant No. DMR 1607139.

- [1] C. S. Wang, M. R. Norman, R. C. Albers, A. M. Boring, W. E. Pickett, H. Krakauer, and N. E. Christensen, Fermi surface of UPt_3 within the local-density approximation, *Phys. Rev. B* **35**, 7260 (1987).
- [2] W. Ubachs, A. P. J. van Deursen, A. R. de Vroomen, and A. J. Arko, Fermi surface measurements on UPd_3 , *Solid State Commun.* **60**, 7 (1986).
- [3] J. von Neumann and E. P. Wigner, On the behavior of eigenvalues in adiabatic processes, *Phys. Z.* **30**, 467 (1929), translated in R. S. Knox and A. Gold, *Symmetry in the Solid State* (Benjamin, New York, 1964), p. 167.
- [4] H. A. Jahn and E. Teller, Stability of polyatomic molecules in degenerate electronic states. I. Orbital degeneracy, *Proc. R. Soc. A* **161**, 220 (1937).
- [5] W. C. Herring, *On Energy Coincidences in the Theory of Brillouin Zones* (Lancaster Press, Lancaster, PA, 1937).
- [6] W. C. Herring, Accidental degeneracy in the energy bands of crystals, *Phys. Rev.* **52**, 365 (1937).
- [7] R. E. Peierls, in *Quantum Theory of Solids*, (Oxford University Press, Oxford, 1955), p. 108.
- [8] X. Wan, A. M. Turner, A. Vishwanath, and S. Y. Savrasov, Topological semimetal and Fermi-arc surface states in the electronic structure of pyrochlore iridates, *Phys. Rev. B* **83**, 205101 (2011).
- [9] P. B. Allen, What happens to geometric phase when spin-orbit interactions lift band degeneracies? [arXiv:0709.1457](https://arxiv.org/abs/0709.1457) (2007).
- [10] P. B. Allen and W. E. Pickett, Accidental degeneracy in k-space, geometrical phase, and the perturbation of π by spin-orbit interactions, *Physica C* **549**, 102 (2018).
- [11] J. R. Badger, Y. Quan, M. C. Staab, S. Sumita, A. Rossi, K. P. Devlin, K. Neubauer, J. C. Fettinger, P. Klavins, S. M. Kauzlarich, D. Aoki, I. M. Vishik, W. E. Pickett, and V. Taufour, Dirac lines and loop at the Fermi level in the time-reversal symmetry breaking superconductor LaNiGa_2 , *Commun Phys* **5**, 22 (2022).
- [12] V. A. Romaka, Yu. N. Grin, Ya. P. Yarmolyuk, R. V. Skolozdra, and A. A. Yartys, Magnetic and Crystallographic Characteristics of RNiGa_2 compounds (R=rare-earth metal), *Ukrainskii Fizicheskii Zhurnal* **28**, 227 (1983).
- [13] A. D. Hillier, J. Quintanilla, B. Mazidian, J. F. Annett, and R. Cywinski, Nonunitary triplet pairing in the centrosymmetric superconductor LaNiGa_2 , *Phys. Rev. Lett.* **109**, 097001 (2012).
- [14] S. K. Ghosh, G. Csire, P. Whittlesea, J. F. Annett, M. Gradhand, B. Újfalussy, and J. Quintanilla, Quantitative theory of triplet pairing in the unconventional superconductor LaNiGa_2 , *Phys. Rev. B* **101**, 100506(R) (2020).
- [15] A. Leonhardt, M. M. Hirschmann, N. Heinsdorf, X. Wu, D. H. Fabiani, and A. P. Schnyder, Symmetry-enforced topological band crossings in orthorhombic crystals: Classification and materials discovery, *Phys. Rev. Materials* **5**, 124202 (2021). See especially Sec. VI. For SG 63.
- [16] Y. Hinuma, T. Hatakeyama, Y. Kumagai, L. A. Burton, H. Sato, Y. Muraba, S. Iimura, H. Hiramatsu, I. Tanaka, H. Hosono, and F. Oba, Discovery of earth-abundant nitride semiconductors by computational screening and high-pressure synthesis, *Nat. Commun.* **7**, 11962 (2016).
- [17] K. Schwarz and P. Blaha, Solid state calculations using WIEN2k, *Comput. Mater. Sci.* **28**, 259 (2003).
- [18] D. J. Singh, Electronic structure and fermiology of superconducting LaNiGa_2 , *Phys. Rev. B* **86**, 174507 (2012).
- [19] I. Hase and T. Yanagisawa, Origin of superconductivity in layered centrosymmetric LaNiGa_2 , *J. Phys. Soc. Jpn.* **81**, 103704 (2012).
- [20] H. M. Tütüncü and G. P. Srivastava, Origin of superconductivity in layered centrosymmetric LaNiGa_2 , *Appl. Phys. Lett.* **104**, 022603 (2014).
- [21] A. A. Burkov, M. D. Hook, and L. Balents, Topological nodal semimetals, *Phys. Rev. B* **84**, 235126 (2011).
- [22] Y. Quan, Z. P. Yin, and W. E. Pickett, A Single Nodal Loop of Accidental Degeneracies in Minimal Symmetry: Triclinic CaAs_3 , *Phys. Rev. Lett.* **118**, 176402 (2017).
- [23] V. Pardo and W. E. Pickett, Electron confinement, orbital ordering, and orbital moments in d^0 - d^1 oxide heterostructures, *Phys. Rev. B* **81**, 245117 (2010).
- [24] M. V. Berry, Quantal phase factors accompanying adiabatic changes, *Proc. R. Soc. Lond A* **392**, 45 (1984).
- [25] M. V. Berry, Aspects of degeneracy, in *Chaotic Behavior in Quantum Systems*, edited by G. Casati (Plenum, New York, 1985), pp. 123-140.
- [26] C. Pfleiderer, Superconducting phases of f -electron compounds, *Rev. Mod. Phys.* **81**, 1551 (2009).
- [27] D. J. Scalapino, A common thread: The pairing interaction for unconventional superconductors, *Rev. Mod. Phys.* **84**, 1383 (2012).
- [28] J. Bardeen, L. N. Cooper, and J. R. Schrieffer, Microscopic theory of superconductivity, *Phys. Rev.* **106**, 162 (1957).
- [29] J. Bardeen, L. N. Cooper, and J. R. Schrieffer, Theory of superconductivity, *Phys. Rev.* **108**, 1175 (1957).
- [30] P. M. Marcus and V. L. Moruzzi, Stoner model of ferromagnetism and total-energy band theory, *Phys. Rev. B* **38**, 6949 (1988).
- [31] J. F. Janak, Uniform susceptibilities of metallic elements, *Phys. Rev. B* **16**, 255 (1977).
- [32] U. Krey, Micromagnetic theory of ferromagnetic superconductors, *Intl. J. Magn.* **3**, 65 (1972).
- [33] Z. F. Weng, J. L. Zhang, M. Smidman, T. Shang, J. Quintanilla, J. F. Annett, M. Nicklas, G. M. Pang, L. Jiao, W. B. Jiang, Y. Chen, and F. Steglich, and H. Q. Yuan, Two-Gap Superconductivity in LaNiGa_2 with Nonunitary Triplet Pairing and Even Parity Gap Symmetry, *Phys. Rev. Lett.* **117**, 027001 (2016).
- [34] X. Dai, Z. Fang, Y. Zhou, and F.-C. Zhang, Even Parity, Orbital Singlet, and Spin Triplet Pairing for Superconducting $\text{LaFeAsO}_{1-x}\text{F}_x$, *Phys. Rev. Lett.* **101**, 057008 (2008).
- [35] J. L. Lado and M. Sgrist, Detecting nonunitary multi-orbital superconductivity with Dirac points at finite energies, *Phys. Rev. Res.* **1**, 033107 (2019).
- [36] M. E. Simon and C. M. Varma, Detection and Implications of a Time-Reversal Breaking State In Underdoped Cuprates, *Phys. Rev. Lett.* **89**, 247003 (2002).
- [37] V. Scagnoli, U. Staub, Y. Bodenthin, R. A. de Souza, M. Garcia-Fernandez, M. Garganourakis, A. T. Boothroyd, D. Prabhakaran, and S. W. Lovesey, Observation of orbital currents in CuO , *Science* **332**, 696 (2011).
- [38] C. Platt, R. Thomale, C. Honerkamp, S.-C. Zhang, and W. Hanke, Mechanism for a pairing state with time-reversal symmetry breaking in iron-based superconductors, *Phys. Rev. B* **85**, 180502(R) (2012).